Journal of ELECTRONIC MATERIALS, Vol. 48, No. 10, 2019
https://doi.org/10.1007/s11664-019-07468-0
© 2019 The Minerals, Metals & Materials Society

First-Principles Study of Strain Engineered Electronic Properties of GeSe-SnS Hetero-bilayer

SHAHNEWAZ AHMED,[1,2] TOWSIF TAHER,[1,3] RAJAT CHAKRABORTY,[1,4] and SAMIA SUBRINA[1,5,6]

1.—Department of Electrical and Electronic Engineering, Bangladesh University of Engineering and Technology, Dhaka 1205, Bangladesh. 2.—e-mail: ahmed.shahnewaz16@gmail.com. 3.—e-mail: towsiftaher@eee.buet.ac.bd. 4.—e-mail: rajat@eee.buet.ac.bd. 5.—e-mail: samiasubrina@eee.buet.ac.bd. 6.—e-mail: ssubr002@ucr.edu

Vertical stacking of two dimensional (2D) materials is emerging as an exciting method for the design of next generation electronic and optoelectronic devices. Here, we employed first-principles calculations based on density functional theory to study the structural and electronic properties of the GeSe-SnS Van der Waals hetero-bilayer. Our results suggest that this hetero-bilayer is semiconducting in nature with a direct band gap of 0.9006 eV and also has an intrinsic type-II band alignment indicating an expectation for spontaneous electron-hole charge separation. The electronic responses of the hetero-bilayer are found to be sensitive and anisotropic to the applied strain. The direct band gap of the GeSe-SnS hetero-bilayer is tunable by strain within a considerable range (0.306–1.197 eV) and the transitions between direct–indirect band gap can repeatedly be obtained by applying compressive uniaxial and biaxial strains. The carrier effective masses of the hetero-bilayer can also be engineered by strain in a low mass range. These intriguing results suggest GeSe-SnS hetero-bilayer as a good candidate for applications in electronic and optoelectronic semiconductor devices.

Key words: Group IV monochalcogenides, hetero-bilayer, strain, electronic properties

INTRODUCTION

Atomically thin two-dimensional (2D) materials have incited immense interest among the researchers due to their distinct characteristics originating from their unique structure and quantum size effects. After the first isolation of graphene,[1] a large number of 2D materials such as hexagonal boron nitride (h-BN),[2] transition metal dichalcogenides,[3] phosphorene [4], etc., have been successfully fabricated in the recent years which illustrate noteworthy electronic, optical and mechanical properties for nanoscale applications.[5] Modulation of their properties by using strain, electric field, doping, multilayers, etc., has always been a topic of extensive investigation as it yields opportunities for a wide range of applications. Formation of van der Waals (vdW) heterobilayer to augment the individual advantages[6–8] has also intrigued the curiosity of many researchers.

Of late, great interest has been drawn into the 2D properties of Group IV monochalcogenides (SnS, SnSe, GeS, GeSe) that include valley dependent transport excited by linearly polarized light,[9] reversible in-plane anisotropy switching by strain or electric field,[10] photostriction[11] and large bulk photovoltaic effect[12] etc. They are isoelectronic to phosphorene with similar orthorhombic puckered structure.[13] Theoretical calculations have shown

(Received January 11, 2019; accepted July 20, 2019; published online August 6, 2019)
S. Ahmed, T. Taher and R. Chakraborty: These authors contributed equally to the work.

strong quantum confinement effect,[14] giant piezoelectricity and in plane ferroelectricity,[15–17] and spin orbital splitting (19–86 meV) due to breaking of inversion symmetry in a monolayer.[13,15] Among the members of this family, monolayer SnS and GeSe have shown great potential for applications in optoelectronic and thermoelectric devices. SnS shows layer dependent anisotropic properties[15] while GeSe is a tunable direct band gap material with small carrier effective mass.[16] The literature also reported the presence of strongly bound Mott–Wannier excitons in a GeSe monolayer.[18] Both monolayer SnS and GeSe are intrinsic multiferroic materials with small thermal conductivity and high electrical conductivity indicating potential application in information storage[16,17] and thermoelectric devices.[19] Anisotropic electronic properties of both materials have been reported to be modulated by strain.[16,20] Moreover, monolayer and few layer SnS and GeSe have been experimentally fabricated using liquid phase exfoliation and physical vapor transport.[21–23] Furthermore, the lattice mismatch between monolayer SnS and GeSe is less than 2.5% [10] which is a minimum among all the combinations of Group IV monochalcogenides. All these promising properties compel the exploration of the vdW hetero-bilayer composed of monolayer SnS and GeSe. Xia et al. Ref. 24 have analyzed the properties of this bilayer with a few orientations (interaction between the atoms of same group in two different layers) but the effect of interactions of Group IV to Group VI atoms of two different layers if they are placed in proximity is yet to be explored. In this article, using first principles calculations, we obtain the stable equilibrium geometry of GeSe-SnS hetero-bilayer and investigate their electronic properties and the effect of strain on it with Perdrew-Burke-Ernzerhof (PBE) calculations.

SIMULATION METHOD

First-principles calculations are performed within the framework of density functional theory[25] using the Quantum Espresso package.[26] The exchange-correlation energy is described by the generalized gradient approximation (GGA) using a PBE[27] functional. A non-local vdW density functional in the form of Beck88 optimization (optB88)[28] is considered for structural optimization to precisely model the dispersive forces between the atomic sheets. It is reported that optB88 gives better predictions for graphene-metal interfaces[29] and layered compounds such as chromium trihalides.[30] The wave functions are expanded in a plane wave basis with a cutoff energy of 40 Ry. The first Brillouin zone (BZ) is sampled with a fine $16 \times 16 \times 1$ Monkhorst-Pack (MP)[31] grid. The geometric structure are optimized with an energy and force convergence threshold of 10^{-6} Ry/atom and 10^{-4} Ry/Bohr, respectively. The thickness of the vacuum region is kept 15Å to avoid interaction due to periodic images.

STRUCTURAL AND ELECTRONIC PROPERTIES OF GeSe-SnS HETERO-BILAYER

Four different stacking patterns, namely AA, AB, AC and AD stacking as shown in Fig. 1(a)–1(d), are considered as such that the group IV atoms in the upper layer are always in close proximity to the group VI atoms in the bottom layer and vice versa. For AA stacking, the top GeSe layer is directly stacked on the bottom the SnS layer (Fig. 1a). In AB stacking, the top GeSe layer is shifted by half unit cell along a(zigzag) direction (Fig. 1b) and as a result the edge of the puckered hexagon of the top layer is located in the center of the puckered hexagon of the bottom layer. For AC stacking, the top and bottom layers are mirror images of each other (Fig. 1c). AD stacking is a half unit cell shifted stacking where the top and bottom layers are mirror images of each other (Fig. 1d). The proposed structures AA, AB, AC, AD are different from the structures proposed by Xia et al. Ref. 24 where atoms of similar groups from two different layers are in close proximity. The unit cell of GeSe-SnS hetero-bilayer contains eight atoms including two Ge, 2 Se, 2 Sn and two S atoms keeping the primitive unit cell of each monolayer to be the same. Total energy calculations for structural optimization based on optB88 indicate that the total energy of AD stacking is more than 10 meV/atom lower than that of AA, AB and AC stacking, making it the most energetically favorable structure. Therefore, AD stacking is considered to be the optimal stacking for the group IV- group VI hetero-bilayer and further studies are done on this stacking. The calculated optimal lattice parameters of GeSe-SnS hetero-bilayer are $a = 4.21$Å and $b = 4.02$Å with equilibrium distance $d = 3.35$Å between the layers as shown in Fig. 1(e). For the benchmarking of our calculation, our computed lattice parameters of monolayer GeSe ($a = 4.26$Å and $b = 3.95$Å) and SnS ($a = 4.21$Å and $b = 4.002$Å) are in good agreement with Gomes et al. Ref. 13 and the obtained results also indicate small lattice mismatch between the monolayers and optimal stacking. For better assessment of the stability of the hetero-bilayer, we calculate the binding energy (E_b) with optB88 calculation using the formula,

$$E_b = E_{\mathrm{GeSe-SnS}} - E_{\mathrm{GeSe}} - E_{\mathrm{SnS}}, \quad (1)$$

where $E_{GeSe-SnS}$ is the total energy of the GeSe-SnS hetero-bilayer per atom, E_{GeSe} and E_{SnS} are the total energies of monolayer GeSe and SnS per atom, respectively. The calculated binding energy at equilibrium interlayer distance of $d = 3.05$Å is found to be -126.83 meV/atom. Our studied hetero-bilayer configuration is suggested to be stable as other similar vdW systems like phosphorene-graphene hetero-bilayer (-71 meV/atom), hexagonal boron nitride-phosphorene hetero-bilayer (-79 meV/atom)[32] and GeSe-phosphorene hetero-bilayer (-18

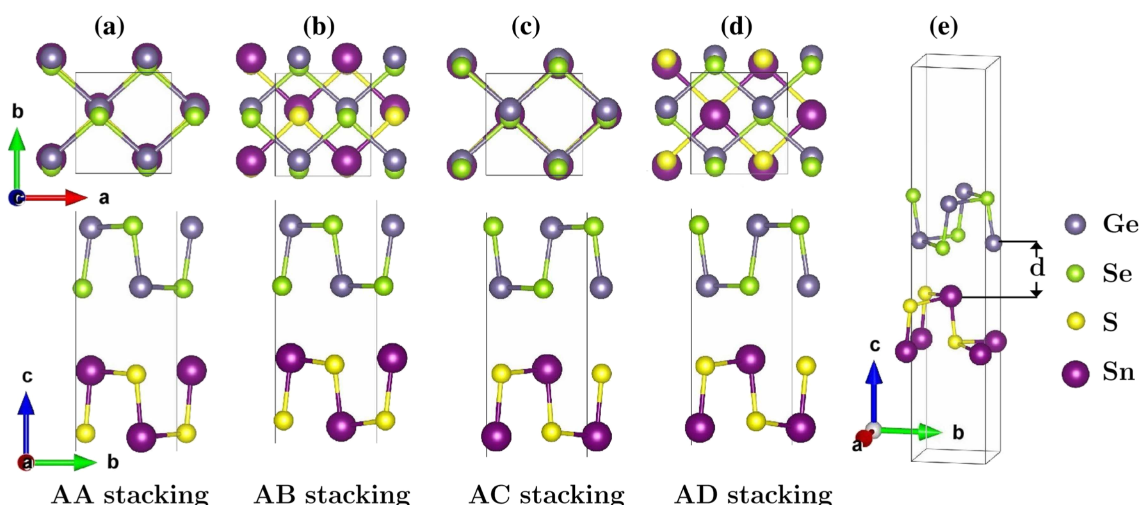

Fig. 1. (a)–(d) Top (top) and side views (bottom) of AA, AB, AC, AD stackings of GeSe-SnS hetero-bilayer, (e) unit cell of optimal stacking of GeSe-SnS hetero-bilayer.

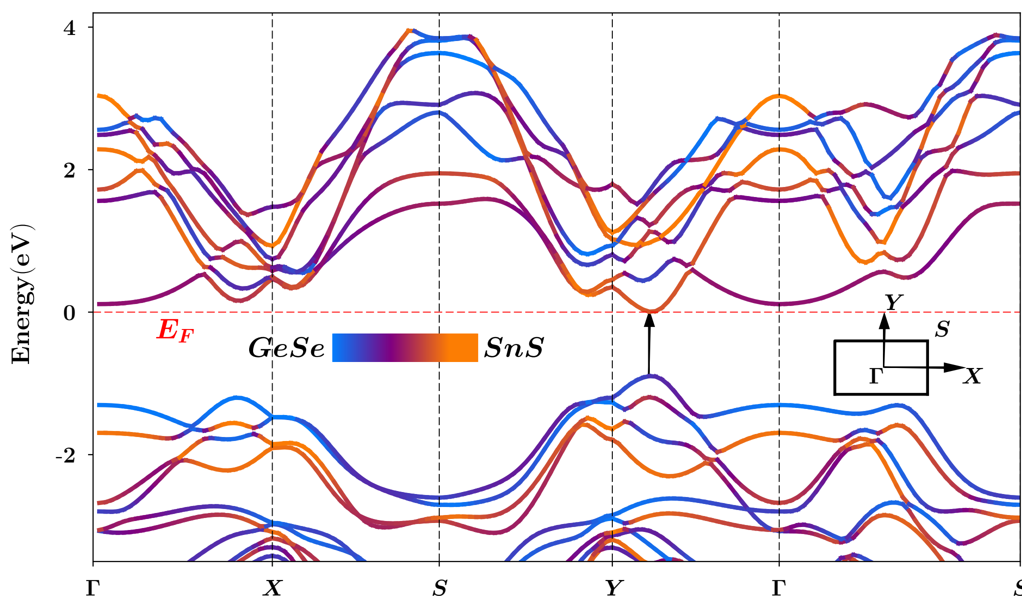

Fig. 2. Projected band structure of GeSe-SnS hetero-bilayer.

meV/atom)[33] that are reported to have binding energy greater than −100 meV/atom.

In this work, projected band structure and density of states (DOS) are calculated using PBE functional. Figure 2 shows the projected band structure of GeSe-SnS hetero-bilayer. GeSe-SnS hetero-bilayer exhibits direct band gap of 0.9006 eV whereas the band gaps of monolayer GeSe and SnS are found to be 1.18 eV and 1.39 eV, respectively, which are in agreement with previous theoretical predictions.[13] Both conduction band minimum (CBM) and valance band maximum (VBM) for hetero-bilayer lie along $\Gamma - Y$ direction and CBM is composed of about 83% GeSe and 17% SnS while VBM is composed of about 29% GeSe and 71% SnS. Similar results were also reported by Xia et al.[24] which predicted direct bandgap for their proposed structure. To better investigate the underlying mechanism of orbital re-configuration of GeSe-SnS hetero-bilayer, the total and projected density of states (PDOS) are plotted in Fig. 3(a). PDOS of GeSe-SnS hetero-bilayer shows that below the Fermi level, p orbitals of S and Se provide major contribution to the total DOS while p orbitals of Sn and Ge contribute significantly to the total DOS above the Fermi level. The overall electronic structure of the GeSe-SnS hetero-bilayer has been formed by overlapping the *p* orbitals of the constituent atoms and thus causes the lowering of the band gap of the hetero-bilayer compared to the band gap of both the monolayers. The quantum confinement in 2D materials due to the removal of the

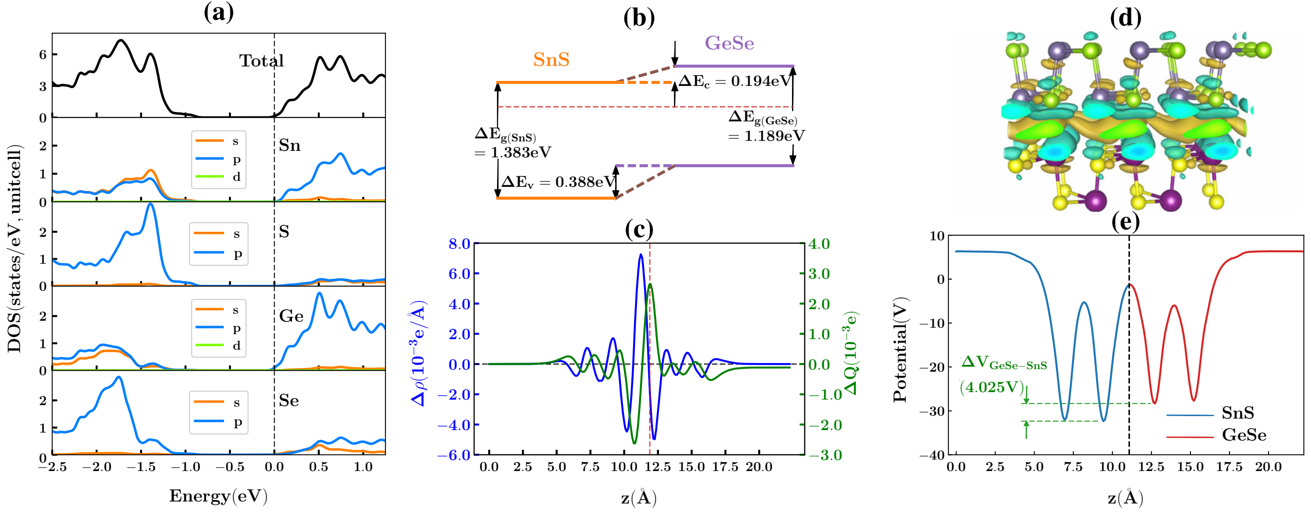

Fig. 3. (a) The DOS and PDOS of GeSe-SnS hetero-bilayer. (b) The band alignment. (c) The planar-averaged differential charge density $\rho(z)$ of the GeSe-SnS hetero-bilayer, along with the amount of transferred charge $Q(z)$ along the normal direction of the surface. (d) Side view of the isosurface of DCD at isovalue 0.00035 e/(Å)^3. Cyan (golden) depicts depletion (accumulation) of charge. (e) The plane averaged electrostatic potential across the interface of the GeSe-SnS hetero-bilayer.

interaction of the p orbitals across the interlayer region generally increases the gap.[34] Hence, the increased overlap in p orbitals explains the decrease in band gap of the hetero-bilayer with vertical stacking of monolayers.

The band alignments of GeSe-SnS hetero-bilayer are investigated in Fig. 3(b) using the vacuum energy level as reference. As shown in the figure, GeSe and SnS layers form type II band alignment with band edges of monolayer GeSe and SnS located at $(-1.064, -2.253)$ eV and $(-1.258, -2.641)$ eV, respectively. Type II band alignment was also found in the study by Xia et al. Ref. 24 This indicates spontaneous separation of electron-hole pairs at the lowest energy level, marking possible application of the hetero-bilayer in optoelectronic devices.

To better understand the charge redistribution at the hetero-bilayer surface, differential charge density (DCD) $\Delta\rho(z)$ along the direction normal to the surface is calculated from in-plane DCD using the formula,

$$\Delta\rho(z) = \int \rho(x,y,z)dxdy - \int \rho_{GeSe}(x,y,z)dxdy - \int \rho_{SnS}(x,y,z)dxdy \quad , \quad (2)$$

where $\rho(x,y,z)$, $\rho_{GeSe}(x,y,z)$,and $\rho_{SnS}(x,y,z)$ are the charge density at (x, y, z) point in GeSe-SnS hetero-bilayer, monolayer GeSe and SnS unit cells, respectively. Here x, y and z are taken along a, b and c directions, respectively. To obtain the amount of transferred charge, cumulative DCD $\Delta Q(z)$ is calculated as given by,

$$\Delta Q(z) = \int_{-\infty}^{z} \Delta\rho(z')dz' \quad (3)$$

$\Delta\rho(z)$ and $\Delta Q(z)$ are plotted in Fig. 3(c). The figure shows that electrons are transferred from GeSe layer to SnS layer leading to p doping in GeSe and n-doping in SnS. This observation is supported by the band diagram in Fig. 3(b) and also by the isosurface of DCD plotted in Fig. 3(d) where accumulation and depletion of electron across the interface are depicted.

The plane-averaged electrostatic potential along the perpendicular direction of GeSe-SnS hetero-bilayer surface is plotted in Fig. 3(e). The work function of GeSe-SnS structure is 2.753 eV while the calculated value of the potential drop across the hetero-bilayer is 4.025V. This potential difference is higher than that of phosphorene/h-BN (3.59V) and lower than those of phosphorene/graphene (6.42V)[32] and GeSe/phosphorene (5.94V),[33] implying the existence of reasonable electrostatic field at the interface. As a result, electron-hole recombination would be altered in both GeSe and SnS.

Next, the carrier effective masses are calculated from the band structure of GeSe-SnS hetero-bilayer according to the equation, $m^* = \hbar^2/(\frac{\partial^2 E}{\partial k^2})$. It can be observed from Table I that the values of carrier effective masses of GeSe-SnS hetero-bilayer are comparable to those of monolayer SnS ($m_e^* = 0.19m_o$, $m_h^* = 0.22m_o$, armchair direction; $m_e^* = 0.20m_o$, $m_h^* = 0.27m_o$, zigzag direction)[35] while smaller than those of monolayer GeSe ($m_e^* = 0.31m_o^*$, $m_h = 0.38m_o$)[36] and phosphorene ($m_e^* = 1.24m_o$, $m_h^* = 4.29m_o$, zigzag direction).[37] Here m_0, m_e^* and m_h^* represent the invariant mass of electron, effective mass of electron and effective mass of hole respectively.

STRAIN EFFECT ON PROPERTIES OF GeSe-SnS HETERO-BILAYER

Figure 4(a) shows total energy as a function of strain based on PBE calculation. GeSe-SnS hetero-bilayer requires less than 83.28 meV/atom to be expanded or compressed by 6%. As the desired strain and harmonic behavior are achievable in elastic regime and at a low energy cost, strain engineering is effective for this hetero-bilayer. The figure shows that effect of strain is more prominent for biaxial compressive strain due to the reduction of the unit cell volume, resulting in the reduced distance between individual atoms. This, in effect, reduces system stability and increases total energy more rapidly for compressive strain.

The variation in band gap under applied strain of varying percentage is depicted in Fig. 4(b). The figure shows that the band gap decreases from 0.9006 eV to 0.4634 eV when GeSe-SnS hetero-bilayer structure is compressed along a axis (zigzag direction) up to 6% and increases to 0.98 eV when it is stretched up to 6%. For strain along b axis (armchair direction), band gap is lowered to 0.79 eV for 6% compressive strain and rises as high as 1.07 eV for 6% tensile strain. Biaxial strain follows the similar trend and the highest achieved band gap is 1.19 eV for 6% tensile strain. The figure concludes that the band gap exhibits a decreasing trend when compressive strain is exerted on the hetero-bilayer and the opposite happens when tensile strain is applied. Furthermore, results also indicate direct-indirect transition of band gap for specific range of applied strain. GeSe-SnS hetero-bilayer shows indirect band gap for more than or equal to 2% of compressive biaxial and uniaxial strain along a axis. On the other hand, the band gap remains direct up to 4% compressive strain and becomes indirect for 6% compressive strain along b axis which is depicted in Fig. 5. Our study finds that band gap remains direct for the applied tensile strain. In case of direct band gap both CBM and VBM are located along the $\Gamma - Y$ direction. However, for indirect band gap cases, we observe that VBM stays in the same position but CBM shifts to Γ point as shown in Fig. 5. This type of high strain tenability makes GeSe-SnS hetero-bilayer structure a promising material for flexible electronics and optoelectronics. Besides this property, it is clear from Fig. 5 that the hetero-bilayer becomes degenerate when compressive biaxial strain is applied.

Table I. Calculated carrier effective masses for GeSe-SnS hetero-bilayer along armchair (along b axis) and zigzag directions (along a axis)

	Armchair	Zigzag
m_e	$0.224m_0$	$0.236m_0$
m_h	$0.268m_0$	$0.213m_0$

Effect of strain on electron and hole effective masses along different directions are shown in Figs. 4(c) and (d). It is observed that effective mass is sensitive to strain and anisotropic due to the characteristic puckered structure. Figures show that effective mass varies over a large range from $0.10006m_o$ to $3.519m_o$ and both electron and hole effective masses are small (in between $0.21m_o - 0.56m_o$) for applied tensile strain. However, in case of applied compressive strain CBM position changes to Γ point where curvature is small and results in a drastic increase of electron effective mass. On the other hand, as VBM holds over the same position, hole effective mass remains small.

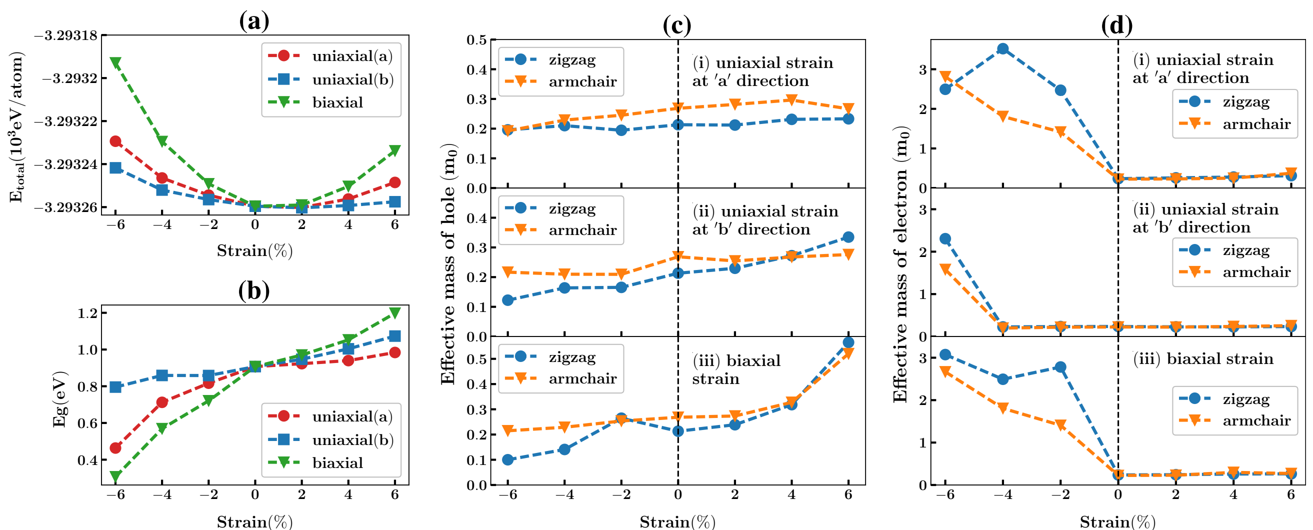

Fig. 4. (a) Total energy, (b) band gap, (c) hole effective mass and (d) electron effective mass (along armchair and zigzag direction) of GeSe-SnS hetero-bilayer as a function of strain, from −6% to 6%.

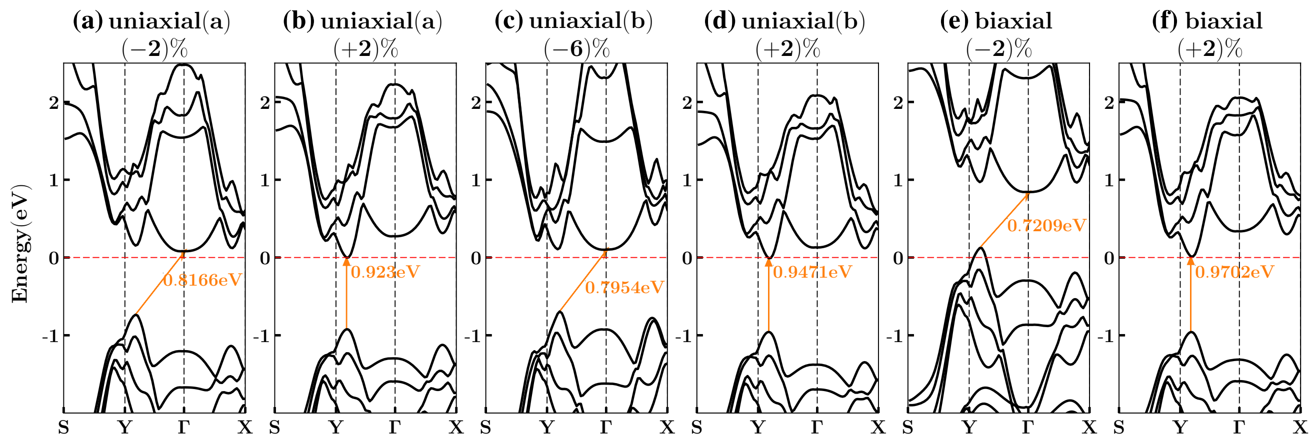

Fig. 5. Band structures of GeSe-SnS hetero-bilayer under uniaxial strain of (a) −2%, (b) +2% along a axis, under uniaxial strain of (c) −6%, (d) +2% along b axis and under biaxial uniform strain of (e) −2%, (f) +2%.

This strain effect can be easily caused by a lattice mismatch on the substrate or mechanical loading.[37,38] As a result, effect of strain on carrier effective mass and band gap may act as an important criterion for the choice of substrate for GeSe-SnS hetero-bilayer.

CONCLUSION

In conclusion, we have investigated the equilibrium geometry and electronic properties of a GeSe-SnS hetero-bilayer from DFT studies considering Van der Waals interaction between two layers. The study shows that a GeSe-SnS hetero-bilayer is a direct band gap semiconductor with type II band alignment. Significant redistribution of charge and potential are observed across the interface and the hetero-bilayer is found to have small anisotropic effective masses which are maintained under the application of tensile strain. Band gap is also strain tunable and direct to indirect transition is observed for a specific range of compressive strain. These results imply that a GeSe-SnS hetero-bilayer would further encourage the application of monochalcogenides in the next generation electronic and optoelectronic devices.

CONFLICT OF INTEREST

The authors declare that there are no conflicts of interest.

REFERENCES

1. K.S. Novoselov, A.K. Geim, S.V. Morozov, D. Jiang, Y. Zhang, S.V. Dubonos, I.V. Grigorieva, *Science* 306(5696), 666 (2004).
2. L. Wang, B. Wu, J. Chen, H. Liu, P. Hu and Y. Liu, *Adv. Mater.* 26(10), 1559 (2014).
3. Q.H. Wang, K. Kalantar-Zadeh, A. Kis, J.N. Coleman and M.S. Strano, *Nat. Nanotechnol.* 7(11), 699 (2012).
4. H. Liu, A. Neal, Z. Zhu, Z. Luo, X. Xu, D. Tománek, P. Ye, Li, Y. Yu, G.J. Ye, Q. Ge, X. Ou, H. Wu, D. Feng, X.H. Chen and Y. Zhang, *Nat. Nano* 9, 372 (2014).
5. G.R. Bhimanapati, Z.M. Lin, V. Meunier, Y. Jung, J.J. Cha, S. Das, D. Xiao, Y. Son, M.S. Strano, V.R. Cooper, L. Liang, S.G. Louie, E. Ringe, W. Zhou, S. Kim, R.R. Naik, B.G. Sumpter, H. Terrones, F. Xia, Y. Wang, J. Zhu, D. Akinwande, N. Alem, J.A. Schuller, R.E. Schaak, M. Terrones and J.A. Robinson *ACS Nano* 9(12), 11509 (2015).
6. G. Giovannetti, P.A. Khomyakov, G. Brocks, P.J. Kelly and J. Van Den Brink, *Phys. Rev. B* 76(7), 073103 (2007).
7. D. Pierucci, H. Henck, J.P.C. Ávila, A. Balan, C.H. Naylor, G. Patriarche, Y.J. Dappe, M.G. Silly, F. Sirotti, A.T.C. Johnson, M.C. Asensio and A. Ouerghi *Nano Lett.* 16(7), 4054 (2016).
8. C. Xu, J. Yuan, D. Wang and Y. Mao, *Mater. Res. Express* 6(3), 036305 (2018).
9. A. Rodin, L.C. Gomes, A. Carvalho and A.C. Neto, *Phys. Rev. B* 93(4), 045431 (2016).
10. P.Z. Hanakata, A. Carvalho, D.K. Campbell and H.S. Park, *Phys. Rev. B* 94(3), 035304 (2016).
11. R. Haleoot, C. Paillard, T.P. Kaloni, M. Mehboudi, B. Xu, L. Bellaiche and S. Barraza-Lopez, *Phys. Rev. Lett.* 118(22), 227401 (2017).
12. T. Rangel, B.M. Fregoso, B.S. Mendoza, T. Morimoto, J.E. Moore and J.B. Neaton, *Phys. Rev. Lett.* 119(6), 067402 (2017).
13. L.C. Gomes and A. Carvalho, *Phys. Rev. B* 92(8), 085406 (2015).
14. I. Appelbaum and P. Li, *Phys. Rev. B* 94(15), 155124 (2016).
15. R. Fei, W. Li, J. Li and L. Yang, *Appl. Phys. Lett.* 107(17), 173104 (2015).
16. M. Wu and X.C. Zeng, *Nano Lett.* 16(5), 3236 (2016).
17. R. Fei, W. Kang and L. Yang, *Phys. Rev. Lett.* 117(9), 097601 (2016).
18. L.C. Gomes, P. Trevisanutto, A. Carvalho, A. Rodin and A.C. Neto, *Phys. Rev. B* 94(15), 155428 (2016).
19. A. Shafique and Y.H. Shin, *Sci. Rep.* 7(1), 506 (2017).
20. T. Taher, R. Chakraborty, S. Ahmed and S. Subrina, 10th International Conference on Electrical and Computer Engineering (ICECE) pp. 1–4 (2018).
21. J.R. Brent, D.J. Lewis, T. Lorenz, E.A. Lewis, N. Savjani, S.J. Haigh, G. Seifert, B. Derby and P. OBrien, *J. Am. Chem. Soc.* 137(39), 12689 (2015).
22. Z. Tian, C. Guo, M. Zhao, R. Li and J. Xue, *ACS Nano* 11(2), 2219 (2017).
23. Y. Ye, Q. Guo, X. Liu, C. Liu, J. Wang, Y. Liu and J. Qiu, *Chem. Mater.* (2017).
24. C. Xia, J. Du, W. Xiong, Y. Jia, Z. Wei and J. Li, *J. Mater. Chem. A* 5(26), 13400 (2017).
25. B. Tong and L. Sham, *Phys. Rev.* 144(1), 1 (1966).
26. P. Giannozzi, S. Baroni, N. Bonini, M. Calandra, R. Car, C. Cavazzoni, D. Ceresoli, G. Chiarotti, M. Cococcioni, I. Dabo, A.D. Corso, S. de Gironcoli, S. Fabris, G. Fratesi, R. Gebauer, U. Gerstmann, C. Gougoussis, A. Kokalj, M. Lazzeri, L. Martin-Samos, N. Marzari, F. Mauri, R. Mazzarello, S. Paolini, A. Pasquarello, L. Paulatto,

C. Sbraccia, S. Scandolo, G. Sclauzero, A.P. Seitsonen, A. Smogunov, P. Umari and R.M. Wentzcovitch, *J. Phys. Condensed Mat.* 21(39), 395502 (2009).
27. J.P. Perdew, K. Burke and M. Ernzerhof, *Phys. Rev. Lett.* 77(18), 3865 (1996).
28. A.D. Becke, *Phys. Rev. A* 38(6), 3098 (1988).
29. W.B. Zhang, C. Chen and P.Y. Tang, *J. Chem. Phys.* 141(4), 044708 (2014).
30. W.B. Zhang, Q. Qu, P. Zhu and C.H. Lam, *J. Mater. Chem. C* 3(48), 12457 (2015).
31. H.J. Monkhorst and J.D. Pack, *Phys. Rev. B* 13(12), 5188 (1976).
32. Y. Cai, G. Zhang and Y.W. Zhang, *J. Phys. Chem. C* 119(24), 13929 (2015).
33. W. Yu, Z. Zhu, S. Zhang, X. Cai, X. Wang, C.Y. Niu and W.B. Zhang, *Appl. Phys. Lett.* 109(10), 103104 (2016).
34. X. Han, H. Stewart, S.A. Shevlin, C.R.A. Catlow and Z.X. Guo, *Nano Lett.* 14(8), 4607 (2014).
35. L. Xu, M. Yang, S.J. Wang and Y.P. Feng, *Phys. Rev. B* 95(23), 235434 (2017).
36. Y. Hu, S. Zhang, S. Sun, M. Xie, B. Cai and H. Zeng, *Appl. Phys. Lett.* 107(12), 122107 (2015).
37. X. Peng, Q. Wei and A. Copple, *Phys. Rev. B* 90(8), 085402 (2014).
38. H. Shi, H. Pan, Y.W. Zhang and B.I. Yakobson, *Phys. Rev. B* 87(15), 155304 (2013).

Publisher's Note Springer Nature remains neutral with regard to jurisdictional claims in published maps and institutional affiliations.